Journal of Materials and Electronic Devices 5 (2023) 21-28

Tailoring Optical and Crystal Structural Properties of Bismuth Ferrite Based Nanomaterials via Ion Doping for Enhanced Photocatalytic Activity

Nurvet Kirkgecit[1*], Rabia Kirkgecit[2], Handan Özlü Torun[3], Serhan Urus[2], and Mehmet S. Bozgeyik[1,4*]

[1*] Department of Physics, Faculty of Science, Kahramanmaras Sutcu Imam University, 46050, Kahramanmaras, Turkiye
[2] Department of Chemistry, Facuty of Science, Kahramanmaras Sutcu Imam University, 46050, Kahramanmaras, Turkiye
[3] Department of Energy System Engineering, Kahramanmaras Istiklal University, 46300, Kahramanmaras, Turkiye
[4*] Department of Materials Science and Engineering, Graduate School of Natural and Applied Science, Kahramanmaras Sutcu Imam University, 46050, Kahramanmaras, Turkiye

Bismuth ferrite based Gadolinium (Gd) modified nano crystallite powder was synthesized by the hydrothermal method. The effects of Gd additive on the phase formation, crystal structure, optical properties, and photocatalytic performance were investigated. Crystal structure, crystallite size and phase formation were used to determine by X-ray diffraction (XRD) technique. Additionally, the structural phase formation was also studied by Raman spectroscopy. Average crystallite size, phase and peak analysis were determined using the X' Pert High Score Plus program. According to the XRD peak pattern, it was determined that the structures of the synthesized sample was formed in the polycrystalline $Bi_{25}FeO_{40}$ (Sillenite) phase. The average crystallite sizes of 3 % Gd modified $Bi_{25}FeO_{40}$ sample was calculated as 50 nm. By using absorption edge data, the bandgap value was determined as 1.98 eV. Photocatalytic performance was evaluated in an environment where methylene blue was used as an organic pollutant, by UV-Vis spectrophotometer under a solar simulator. The photocatalytic efficiency was calculated as 70 %. Such a high efficiency was attributed to increased optical absorption, narrowing band gap, thereby, probably the efficient separation and migration of photogenerated charge carriers. It was concluded that although unintentionally formed Sillenite during synthesis of bismuth ferrite is useful for photocatalysis. Furthermore, it was pointed that the optical properties by means of crystal structure is able to be tailored by doping to increase the photocatalytic activity.

Keywords: *Photocatalytic performance, Optical properties, Crystal structural properties, Bismuth ferrite, Sillenite phase*

Submission Date: 15 October 2023
Acceptance Date: 06 December 2023

*Corresponding authors: nurvetkrkgct@gmail.com, msbozgeyik@yahoo.com

1. Introduction

As the environmental and energy problems faced by humanity increase, the material properties needed to solve them also need to improve. Within this theme, the material that scientists adhere to the most are semiconductors [1].

Science and technology-based industry and industrial production have continuously advanced by utilizing both

surface and underground natural resources to meet the growing needs of humanity. However, this process has led

humanity, albeit belatedly, to realize that it has disrupted the balance with nature and there by caused environmental problems. Industrial production and needs based on the usage of limited fossil fuels as an energy source continue significantly, despite their low efficiency and environmental pollution. In this context, while efforts are being made to research and promote alternative, clean, and environmentally friendly renewable energy sources, on the other hand, solutions are being sought to prevent and mitigate environmental pollution and its consequences.

Photocatalysis is the mechanism of creating chemical reactions from light energy. Basically, it is the mechanism of conversion of large chemical compounds harmful to the environment and human health into smaller and harmless chemical compounds and water with the use of electron-hole pair formed by light energy absorption by using a semiconducting material. Semiconductors are unique materials with the ability to generate electron-hole pairs with appropriate light energy. However, on the other hand, the band gaps of semiconductor materials, which have widespread applications in this regard, have wide bandgaps, for example, from 3.3 eV for TiO_2 to 2.67 eV for α-Fe_2O_3. However, the energy range from UV to near UV constitutes only about 5 % of the total solar radiation. For this reason, since other suitable materials have not yet been discovered and brought to the application level for these applications, these materials, which are frequently mentioned in such applications, make photocatalysis impractical.

As a unique single phase room temperature magnetoelectric multiferroic Bismuth Ferrite is a transition metal oxide that includes structural compounds such as perovskite ($BiFeO_3$), mullite ($Bi_2Fe_4O_9$) and sillenite ($Bi_{25}FeO_{40}$). The synthesis of pure $BiFeO_3$ phase in various production methods is challenging, thereby, often results in the formation of secondary phases like Bi_2O_3, Fe_2O_3, $Bi_{25}FeO_{40}$, $Bi_2Fe_4O_9$. Although the presence of these secondary phases may initially create a negative perception, studies have revealed that they actually offer a significant advantage. For instance, the narrow band gap of 1.8 eV in $Bi_{25}FeO_{40}$ makes it a promising material for visible light region applications [2]. On the other hand, it has been stated that $Bi_{25}FeO_{40}$ contributes to electron-hole pair lifetime and recovery in the photocatalytic process due to its superparamagnetic nature [3, 4]. From this point of view, $Bi_{25}FeO_{40}$ as a representative silenite type compound formed unintentionally as a by-product in BFO synthesis could have a potential to show photocatalytic activity for the degradation of organic impurities under visible light irradiation [5].

The current research article evaluates the potential of the photocatalytic performance of Gd modified $Bi_{25}FeO_{40}$ which is intentionally synthesized by hydrothermal method. It was investigated to the performance of the conversion of harmful organic compounds in industrial wastes into harmless inorganic molecules using solar energy, in terms of preventing environmental pollution. For this purpose, the production and application of nano crystallized photocatalyst material has been carried out in order to increase photocatalytic activity and efficiency. Hence, photocatalytic degradation efficiency was discussed on the basis of crystal structure, bandgap, and crystallite size.

2. Experimental

2.1. Preparation of photocatalysts

The synthesis of 3 % Gd modified $Bi_{25}FeO_{40}$ photocatalysts was done by hydrothermal method. Bismuth nitrate [$Bi(NO_3)3.5H_2O$], Iron nitrate [$Fe(NO_3)_3.9H_2O$], Nitric acid (HNO_3), Gadolinium nitrate [$Gd(NO_3)_3.6H_2O$], Potassium nitrate (KNO_3) and Potassium hydroxide (KOH) was used. First, 50 ml of distilled water was diluted with nitric acid. Bismuth nitrate (0.005 mol), Gadalinium nitrate (0. 00015 mol) and Iron nitrate (0. 00485 mol) powders weighed into diluted distilled water were added respectively. After a certain mixing period, a clear solution was observed. 50 ml of 12 M KOH solution was added dropwise with magnetic stirrer until brown precipitate formed. Then the solution was filtered on watman paper and the pH was reduced to 7 by washing with distilled water. The dried powder sample was placed in a glass beaker and 40 ml of KOH was added to it and stirring was continued in the magnetic stirrer. The total solution was transferred to the Teflon container and kept in the hydrothermal device at 200 °C for 24 hours. As a result of the process, it was expected to cool at room conditions. Finally, the obtained product was washed with pure water and the pH was reduced to 7.

Figure 1 shows the general scheme of the hydrothermal method.

Fig.1. Schematic representation of the hydrothermal method process

2.2. Structural Analysis

X-ray Diffraction (XRD) is used to analysis crystal structure by utilizing Philips X'Pert Promodel (λ=0. 154056 nm, Cu-Ka radiation). The average crystallite size calculation of the synthesized catalysts was characterized by using diffraction meter for phase and peak analysis.

2.3. Photocatalytic Measurements

Methylene blue (MB) dye used as an indicator contaminant in water was used. First of all, 5 mg of methylene blue was weighed from the powder sample on a precision digital precision balance and taken into a capped glass tube. After 5 ppm MB + 200 ml distilled water solution was completely dissolved, 10 mg photocatalyst powder sample and 5 ppm MB aqueous solution were suspended in 50 mL aqueous solution. Before illumination, the aqueous solution was kept in the dark for 30 minutes to achieve equilibrium adsorption on the surface of the catalyst. In the measurements, 2 ml samples were taken from the solutions and used. The particulate samples were spun in the centrifuge before the measurement was taken. The Shimadzu UV spectrophotometer (Model: UV-1800) was used to examine the absorbance properties of the solution samples. Measurements were made in the wavelength range of 400 - 800 nm and were repeated every 10 minutes, taking 0 minutes as the starting point. After 120 minutes of measurement, the process was terminated. Methylene blue visible wavelength = 664 nm. The percent photocatalytic degradation of the samples was determined according to the formula below.

$$Degradation\ \% = \frac{C_0 - C_t}{C_0} \times 100 \qquad (1)$$

where C_0 and C_t (mg/l) are the initial and concentration at time t (mg/l). This process was repeated for each sample.

2.4. Forbidden band gap measurement

First of all, 10 mg was weighed from the powder sample on a precision digital precision balance. The weighed sample was taken into a glass tube. Ethyl alcohol was added stoichiometrically on the sample. The ethyl alcohol aqueous solution was mixed in an ultrasonic water bath for about 2 minutes. After the process was completed, measurements were taken using a UV-vis spectrophotometer. Absorption spectrum scanning was taken between 200-900 nm.

3. Results and Discussion

XRD technique is an important structural analysis method to confirm the formation of synthesized compounds (like bulk and nano crystallites) and their degree of crystallization. The mean crystallite size calculation of the samples was analyzed by embedded X'Pert High Score Plus program according to the Debye–Scherrer formula,

$$D_c = {}^{\kappa\lambda}/_{\beta cos\theta} \qquad (2)$$

Where D_C is the mean crystal size, λ is the X-ray wavelength, and β is the width of the diffraction peak at the half-maximum for the diffraction angle (2θ).

Figure 2 shows the XRD diffraction pattern 3 % Gd modified sillenite ($Bi_{25}FeO_{40}$) powder samples prepared by the hydrothermal method.

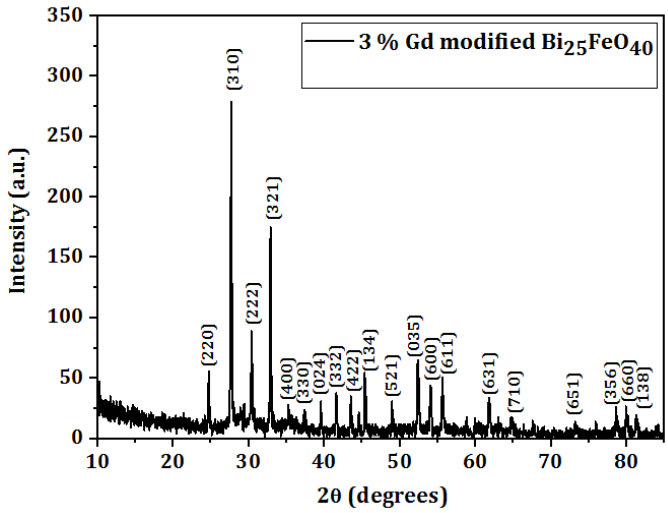

Fig.2. XRD pattern of 3 % Gd modified $Bi_{25}FeO_{40}$ powders prepared by hydrothermal method

The sample was well crystillized in polycrystalline form. By analyzing with the X'Pert High Score Plus program, it was determined that it was formed in the cubic structure $Bi_{25}FeO_{40}$ (Sillenite) phase in the I23 space group. XRD diffraction peaks highly overlap with ICSD card no: 01-078-1543 peaks. The average crystallite size considering using all the diffraction peaks is obtained as 50 nm.

Raman spectroscopy is a highly sensitive technique used to detect atomic displacements, lattice distortions, and phase transitions. This analysis technique is generally used to verify the data obtained from XRD and Rietveld analyzes [6].

Figure 3 shows the Raman scattering spectra of the sample at room temperature.

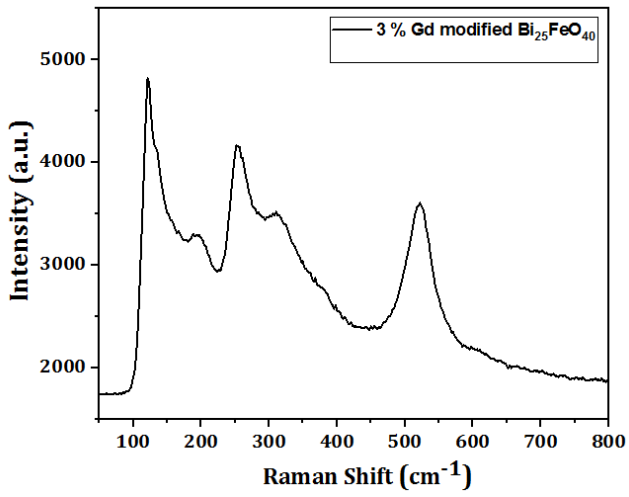

Fig.3. Raman spectra of 3% Gd modified $Bi_{25}FeO_{40}$

The peak intensities are clearly high and expanded. Six main Raman peaks around 140, 200, 250, 320, 520 cm^{-1} were observed. Such modes lower than 400 cm^{-1} are associated with Bi-O covalent bonding, while the higher mode is associated with Fe-O bonds. Raman peaks can be affected by grain size, impurities, lattice distortions, stresses and also defects [7]. The frequencies of the Raman modes can vary depending on the ionic masses. The atomic mass of the Gd^{3+} ion is greater than that of the Fe^{3+} ions. Increasing the ion radius and atomic mass can lead to distortions in the lattice structure affecting the Raman peaks [8].

In the context of optoelectronic applications, the study of optical properties such as absorption edge and band gap energy, which are closely related to each other, is of great importance [9]. The process photocatalysis process start with radiation of the semiconducting catalyst by sunlight or other irradiation sources (for example, ultraviolet lamps or light-emitting diodes) with wavelengths equal to or greater than the forbidden band namely bandgap (E_g) to generate electron-hole pairs. Optical absorption, which is a key factor in the photocatalytic mechanism and constitutes the initial step, is related to the bandgap of a semiconductor. In the photocatalytic process, the photon absorbing capacity of the semiconductor material should be as high as possible so that the electron-hole pairs become more excitable and more electron-hole pairs can be formed. However, this condition can only be met by a narrow bandgap semiconductor material absorbing a wider range of light spectrum [10, 11]. The bandgap value of a semiconductor photocatalysts is extremely important factor which affects the photocatalytic performance. The energy bandgap can be calculated using the Tauc equation given as

$$(\alpha h\vartheta)^2 = A(E_g - h\vartheta)^n \quad (3)$$

[12]. Here, α is the absorption constant and $h\vartheta$ is the energy of the incident photon, E_g refers to the bandgap, and A indicates the scaling constant, while n is a factor dependent on the type of semiconductor material. The exponent 'n' value is 1/2 in indirect band gap semiconductors, while this value is 2 in direct band gap semiconductors.

In order to examine the absorption spectra and determine the band gap value the date were taken in the range of 200-900 nm using a UV-vis spectrophotometer. Figure 4 shows the Tauc plot for band gap calculation.

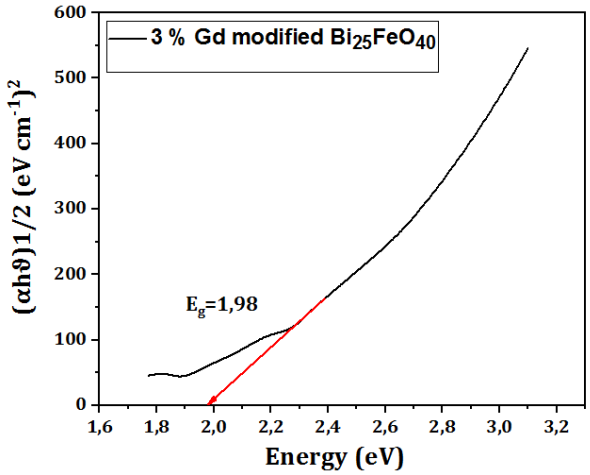

Fig.4. Tauc plot of 3% Gd modified $Bi_{25}FeO_{40}$

The bandgap absorption edge is around 600 nm. The solar radiation energy is in the visible region at a rate of 43% (400-700 nm). It is in the infrared (UV) band greater than >700 nm at a rate of 52 % and in the ultraviolet (IR) (300-400 nm) band at 5%. The wider absorption range means that the 3% Gd modified $Bi_{25}FeO_{40}$ photocatalyst can absorb a greater range of visible light wavelengths. Electrons can be excited from the valence band to the conduction band at wavelengths less than 600 nm. A sharp decrease in the absorption plot of the 3% Gd modified $Bi_{25}FeO_{40}$ may be due to a different light absorption behavior due to different morphology and surface properties [13].

The bandgap was calculated as E_g =1.98 eV using the Tauc plot method as shown in Figure 5. In general, the band gap of semiconductors can vary depending on various factors such as crystal size, changes in lattice parameters, surface morphology, and the presence of additives [14]. The reduced energy band gap is attributed to the reduction in size of the smaller crystallite nanoparticles [15]. Another possible reason for the decrease in the band gap value may be the production of shallower energy band levels as a result of doping instead of Fe [16]. In this context, it is predicted that

with the narrowing of the band gap, the 3 % Gd modified $Bi_{25}FeO_{40}$ photocatalyst will have a positive effect on the photocatalytic activity. Hence, it is expected that the ability of Gd modified $Bi_{25}FeO_{40}$ to benefit from sunlight more effectively will greatly increase [17, 18].

In order to evaluate the photocatalytic degradation capabilities of the synthesized photocatalysts, the pollutant was investigated using methylene blue as a model. At the initial stage, the degradation efficiency of the aqueous solution of the methylene blue dye was tested without the use of any catalyst (photolysis). In the next step, photocatalytic degradation activities of 3 % Gd modified $Bi_{25}FeO_{40}$ was evaluated by examining the photodegradation of methylene blue molecules. Measurements carried out in the wavelength range of 400-800 nm under the solar simulator were made within a period of time starting from 0 minutes to 120 minutes.

Figure 5 shows the absorbance of a catalyst-free methylene blue aqueous solution in daylight in a closed environment without sunlight.

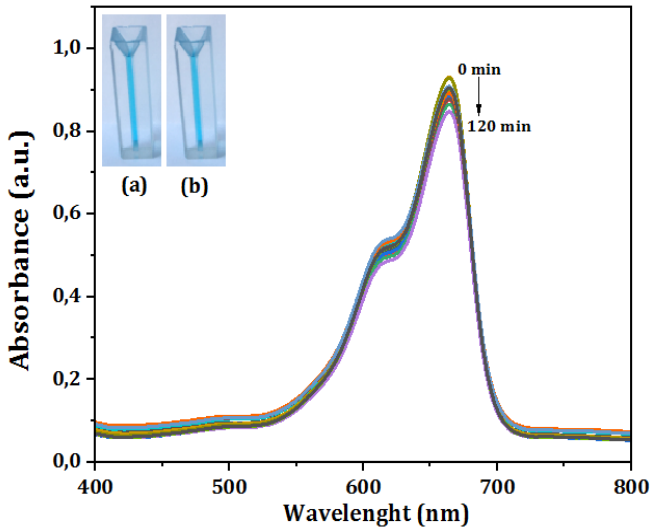

Fig.5. Absorbance plot of an aqueous solution of methylene blue (daylight) without a catalyst

As seen in Figure 5 inset (a) and (b), in the catalyst-free methylene blue aqueous solution, not much change was observed in the measurement from 0 minutes to 120 minutes. In the photocatalytic measurement process that lasted for 120 minutes, an efficiency of 6.74 % was obtained in the methylene blue aqueous solution without catalyst.

Figure 6 shows the absorbance plot of a catalyst-free methylene blue aqueous solution recorded under a solar simulator.

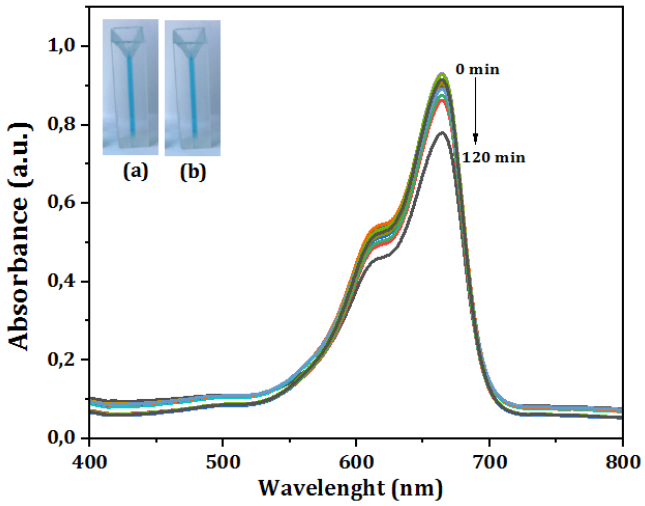

Fig.6. Absorbance plot of an aqueous solution of methylene blue (sunlight) without a catalyst

The photocatalytic degradation efficiency of the aqueous solution of methylene blue without catalyst was calculated as 15% under the solar simulator. This is also the expected situation. In this context, our aim is to compare methylene blue in a solar simulator environment (sunlight) and in a closed environment that does not receive light under normal conditions (daylight).

The main issue for electronic and optical processes in semiconductor material and device applications is that electron-hole pair formation, exciton lifetime and recombination physical measurables are at necessary and sufficient levels [19]. The response to visible light and the effective separation of excited electrons and holes within the photogenerated conduction band are two important parameters for photocatalytic performance [20, 21]. Considering the photocatalytic mechanism, the important problem that negatively affect the initial performance include the low efficiency absorption of visible light, the presence of fast recombination (electron-hole pair recombination) processes, and the low migration capability of photo-generated electrons-hole pairs [22, 23, 24]. The photocatalytic oxidation cycle consists of three basic steps. In the first step, the semiconductor catalyst is excited by sunlight or other irradiation sources (for example, ultraviolet lamps or light-emitting diodes) with wavelengths equal to or greater than the band energy gap. In the second stage, as a result of excitation, the formation of photoactive species (electron-hole pairs) and their transport to the surface of the catalyst occur. The last stage is the formation of oxidation-reduction reactions on the photocatalyst surface. Photogenerated holes in the first stage remain at lower energy levels, while photogenerated electrons jump to higher energy levels. Because they have a short lifetime at high energy levels, electrons rapidly goes back to lower energy

levels and recombine with the holes. This process leads to a reduction in the number of holes and electrons involved in photocatalytic reactions. As a result, the rapid recombination rate of photogenerated electron-hole pairs can inhibit the decomposition of target organic compounds, thus causing a decrease in photocatalytic efficiency [25].

Figure 7 shows the wavelength dependent absorbance plot of the 3 % Gd modified $Bi_{25}FeO_{40}$ photocatalyst.

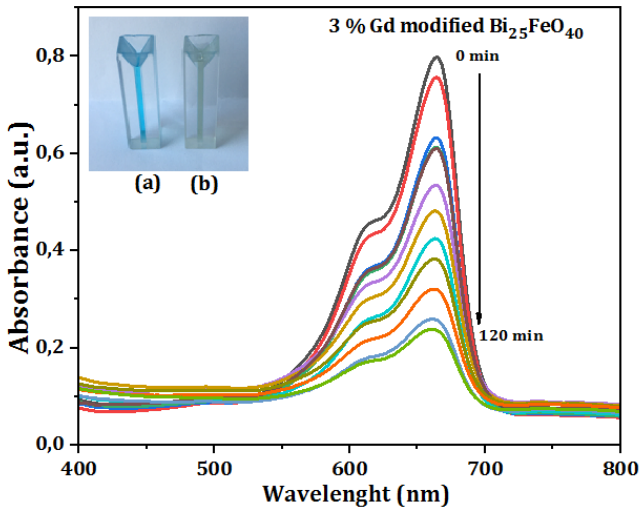

Fig.7. Absorbance plot of 3% Gd modified $Bi_{25}FeO_{40}$ photocatalyst in methylene blue

The figure presents a representation showing the degradation of methylene blue, where the decrease in absorbance density with increasing irradiation time is clearly visible. The percent removal of 3% Gd modified $Bi_{25}FeO_{40}$ photocatalyst on methylene blue dyestuff was calculated from equation 1 as 70%. It can be seen that the photocatalyst exhibits clear photocatalytic behavior. The efficiency and photocatalytic activity of BFO-based semiconductor Nano catalysts are directly affected by many factors such as electronic band structure, surface morphology, crystal size, porosity and surface area that affect the separation of e^{-}-h^{+} pairs and optical absorption properties [26, 27, 28]. Optical absorption is considered a key factor to evaluate the photocatalytic activity of catalysts, and this is closely related to the band gap of the catalyst. The increased photocatalytic efficiency can be attributed to the increased absorption capacity due to the reduced bandgap [29]. At the same time, the improvement in photocatalytic activity may be due to the reduction in recombination of electron-hole pairs by Gd modification [30]. Of these, the improved photocatalytic efficiency may also be due to smaller crystal size, an increase in specific surface areas, resulting in a larger contact area and higher density of active reaction sites [31].

Table 1 shows the crystallite size, photocatalytic activity efficiencies and band gap values of 3% Gd modified $Bi_{25}FeO_{40}$ photocatalysts.

Table1. Crystallite size, bandgap, and photocatalytic activity efficiency.

Photocatalyst	**Crystallite size (nm)**	**Band gap value (eV)**	**Photocatalytic activity yield (%)**
3 % Gd modified $Bi_{25}FeO_{40}$	50	1,98	70

4. Conclusion

In conclusion, 3% Gd modified $Bi_{25}FeO_{40}$ catalyst was synthesized using the hydrothermal method. A decrease in crystallite size was observed depending on the change in experimental parameters. Photocatalysts have been found to exhibit different visible light absorption properties. In addition, the bandgap was calculated as 1.98 eV. The reduction of optical band gap of nano crystallite 3% Gd modified $Bi_{25}FeO_{40}$ shows that it could be a promising material for UV-visible light photocatalysts. These findings reveal that the Gd modification plays a critical role when evaluating their effects on the performance of photocatalysts. As a result, the increase in the photocatalytic activity provides a more effective decomposition due to the emergence of narrowing of the band gap and reduction of the crystal size. From these results, it can be concluded that the doped 3% Gd modified $Bi_{25}FeO_{40}$ nanomaterial has the potential to be developed for photocatalytic applications.

Acknowledgement

The corresponding authors acknowledge Kahramanmaras Sutcu Imam University for the financial support of the postdoctoral research project of DOSAP-2022/5-18.

References

[1] Karataş, Ş., Effect of perylenetetracarboxylic dianhydride on the main electrical properties and interface states of Al/p-Si structures. Physica B: Condensed Matter 657 (2023) 414790.

[2] Li, J., Song, J., Chen, J., Yu, S., Jin, D., & Cheng, J., PVA (Polyvincyl Acohol)-assisted Hydrothermal Preparation of $Bi_{25}FeO_{40}$ and Its Photocatalytic Activity. MRS Online Proceedings Library 1217 (2009) 1-6

[3] Sun, A., Chen, H., Song, C., Jiang, F., Wang, X., & Fu, Y., Magnetic $Bi_{25}FeO_{40}$-graphene catalyst and its high visible-light photocatalytic

performance. RSC Advances 3(13) (2013) 4332-4340

[4] Tan, G. Q., Zheng, Y. Q., Miao, H. Y., Xia, A., & Ren, H. J. Controllable microwave hydrothermal synthesis of bismuth ferrites and photocatalytic characterization. Journal of the American Ceramic Society 95 (1) (2012) 280-289

[5] Zhang, L., Zhang, X., Zou, Y., Xu, Y. H., Pan, C. L., Hu, J. S., & Hou, C. M., Hydrothermal synthesis, influencing factors and excellent photocatalytic performance of novel nanoparticle-assembled $Bi_{25}FeO_{40}$ tetrahedrons. CrystEngComm, 17(34) (2015) 6527-6537

[6] Brahma, S. S., Nanda, J., Sahoo, N. K., Naik, B., & Das, A. A., Phase transition, electronic transitions and visible light driven enhanced photocatalytic activity of Eu–Ni co-doped bismuth ferrite nanoparticles. Journal of Physics and Chemistry of Solids 153 (2021) 110018

[7] Dhanya, S. R., Nair, S. G., Satapathy, J., & Kumar, N. P., Structural and spectroscopic characterization of bismuth-ferrites. In AIP Conference Proceedings 2166 (2019) 1

[8] Bozgeyik, M. S., Kirkgecit, N., Katiyar, R. K., & Katiyar, R. S., Monitoring structural variation on Gd ratio of La modified bismuth ferrite ceramics with enhanced magnetization. Journal of Alloys and Compounds 819 (2020) 153050

[9] Helfi, K., Mousavi Ghahfarokhi, S. E., & Zargar Shoushtari, M., Structural, magnetic, optical, and photocatalytic properties of $Bi_{1-x}Sm_xFe_{1-y}Cr_yO_3$ nanostructure synthesized by hydrothermal method. Applied Physics A 129(1) (2023) 40

[10] Fatima, S., & Rizwan, S., Synergetic Catalytic and Photocatalytic Performances of Tin-Doped $BiFeO_3$/Graphene Nanoplatelet Hybrids under Dark and Light Conditions. ACS omega 8(4) (2023) 3736-3744

[11] Gupta, R., Singh, S. P., Walia, R., Kumar, V., & Verma, V., Modification in photovoltaic and photocatalytic properties of bismuth ferrites by tailoring band-gap and ferroelectric properties. Journal of Alloys and Compounds 908 (2022) 164602

[12] Tauc, J., Grigorovici, R., & Vancu, A, Optical properties and electronic structure of amorphous germanium. physica status solidi (b) 15(2) (1966) 627-637

[13] Hossain, M. S., Palanivel, B., Rokhum, S. L., Selvamani, M., Vadivel, S., Alsulmi, A., ... & Sundaramoorthy, A., Bismuth Ferrite ($BiFeO_3$) 2D-Nanoflakes for the Photocatalytic Degradation of Chromogenic Dyes under Solar Irradiation. Surfaces and Interfaces (2023) 103240

[14] Irfan, S., Liang, G. X., Li, F., Chen, Y. X., Rizwan, S., Jin, J., ... & Ping, F., Effect of graphene oxide nano-sheets on structural, morphological and photocatalytic activity of $BiFeO_3$-based nanostructures. Nanomaterials 9(9) (2019) 1337

[15] Kebede, M. T., Devi, S., Dillu, V., & Chauhan, S., Effects of Sm and Cr co-doping on structural, magnetic, optical and photocatalytic properties of $BiFeO_3$ nanoparticles. Materials Science and Engineering: B 283 (2022) 115859

[16] Nazeer, Z., Bibi, I., Majid, F., Kamal, S., Arshad, M. I., Ghafoor, A., ... & Iqbal, M., Optical, Photocatalytic, Electrochemical, Magnetic, Dielectric, and Ferroelectric Properties of Cd- and Er-Doped $BiFeO_3$ Prepared via a Facile Microemulsion Route. ACS omega (2023).

[17] Zhang, N., Chen, D., Niu, F., Wang, S., Qin, L., & Huang, Y., Enhanced visible light photocatalytic activity of Gd-doped $BiFeO_3$ nanoparticles and mechanism insight. Scientific reports 6(1) (2016) 26467

[18] Maleki, H., Characterization and photocatalytic activity of Y-doped BiFeO3 ceramics prepared by solid-state reaction method. Advanced Powder Technology 30(11) (2019) 2832-2840

[19] Seymen, H., Berk, N., Orak, I., & Karataş, Ş., Effect of illumination intensity on the electrical characteristics of Au//SiO2/n-type Si structures with GO and P3C4MT interface layer. *Journal of Materials Science: Materials in Electronics*, *33*(24), (2022) 19656-19666.

[20] Ghadage, P., Kodam, P., Nadargi, D., Patil, S., Tamboli, M., Bhandari, N., ... & Suryavanshi, S., Pd loaded bismuth ferrite: A versatile perovskite for dual applications as acetone gas sensor and photocatalytic dye degradation of malachite green. Ceramics International 49(4) (2023) 5738-5747

[21] Verma, M. K., Kumar, A., Das, T., Kumar, V., Singh, S., Rai, V. S., ... & Mandal, K. D., $BiFeO_3$ perovskite as an efficient photocatalyst synthesised by soft chemical route. Materials Technology 36(10) (2021) 594-602

[22] Zhou, T., Zhai, T., Shen, H., Wang, J., Min, R., Ma, K., & Zhang, G., Strategies for enhancing performance of perovskite bismuth ferrite photocatalysts ($BiFeO_3$): A comprehensive review. Chemosphere, (2023) 139678

[23] Liu, Y., Yang, B., He, H., Yang, S., Duan, X., & Wang, S., Bismuth-based complex oxides for photocatalytic applications in environmental remediation and water splitting: A review. Science of The Total Environment 804 (2022) 150215

[24] Constantino, D. S., Dias, M. M., Silva, A. M., Faria, J. L., & Silva, C. G., Intensification strategies for improving the performance of photocatalytic processes: A review. Journal of Cleaner Production 340 (2022) 130800

[25] Nazeer, Z., Bibi, I., Majid, F., Kamal, S., Ghafoor, A., Ali, A., ... & Iqbal, M., Microemulsion synthesis of Ga and Sr doped BiFeO3 nanoparticles and evaluation of their ferroelectric, optical, dielectric and photocatalytic properties. Physica B: Condensed Matter 657, (2023) 414788

[26] Irfan, S., Zhuanghao, Z., Li, F., Chen, Y. X., Liang, G. X., Luo, J. T., & Ping, F., Critical review: Bismuth ferrite as an emerging visible light active nanostructured photocatalyst. Journal of Materials Research and Technology 8(6) (2019) 6375-6389

[27] Supriya, S., Recent trends and morphology mechanisms of rare-earth based $BiFeO_3$ nano perovskites with excellent photocatalytic performances. Journal of Rare Earths (2022)

[28] Gao, T., Chen, Z., Huang, Q., Niu, F., Huang, X., Qin, L., & Huang, Y., A review: preparation of bismuth ferrite nanoparticles and its applications in visible-light induced photocatalyses. Rev. adv. mater. Sci 40(2) (2015) 97-109

[29] Dixit, T. K., Sharma, S., & Sinha, A. S. K., Development of heterojunction in N-rGO supported bismuth ferrite photocatalyst for degradation of Rhodamine B. Inorganic Chemistry Communications 117 (2020) 107945

[30] Sahni, M., Kumar, S., Chauhan, S., Singh, M., Pandit, S., Sati, P. C., ... & Kumar, N., Structural, optical and photocatalytic properties of Ni doped $BiFeO_3$ nanoparticles. Materials Today: Proceedings 49 (2022) 3015-3021

[31] Jamaludin, N., Razak, N. A. A., Ismail, F. D., & Chaudhary, K. T., Photocatalytic degradation of rhodamine B dye under visible light using cerium-cobalt co-doped bismuth ferrite nanoparticles. In Journal of Physics: Conference Series 2432 1 (2023) 012015)